Extremely Emissive V-Grooved Microstructure Made of SU-8 for Enhanced Radiative Cooling

Seyed Hossein Hosseini Biuki, Majid Badieirostami, and Mahmoud Shahabadi, *Senior Member, IEEE*

***Abstract*—For a structure to show radiative cooling property, it must have first, high reflectivity of above 90% in the wavelength range of 0.3 to 3 μm, and second, high emissivity for the wavelengths ranging from 8 to 13 μm, namely atmospheric transparency window. Being inspired by the architecture of microwave absorbers used extensively for antenna measurements, we proposed a novel microstructure with near unity emissivity that can be further developed for radiative cooling. To this end, we designed and analyzed a V-grooved multilayer periodic microstructure capable of perfectly emitting in the aforementioned wavelength range. Further, SU-8 is selected as the material of the proposed microstructure. SU-8 is the commonly used material in photolithographic based microfabrication and it is shown, for the first time, that its bulk optical properties are appropriate for radiative cooling purposes. The numerical simulations of the emissivity were performed through a semi-analytical computational technique known as Transmission-Line Formulation (TLF) which enables us to accurately and efficiently calculate electromagnetic radiations reflected from or transmitted through a multilayer structures composed of periodic layers of absorbing materials. It was demonstrated through the simulations that the average emissivity of the proposed microstructure can even exceed 99% in the wavelength range desired for radiative cooling.**

***Index Terms*—Radiative cooling, SU-8 photoresist, transmission line formulation.**

I. Introduction

SEEKING and exploring for cooling techniques by mankind dates back for centuries, long before the invention of electricity, through advanced and harmless use of nature. Wind tower as an outstanding architecture for clean passive cooling traces back to 900 AD in Great Persia where it was aimed for residential cooling [1]. Though because of electric power discovery there is a huge leap forward, recent cooling systems cause environmental concerns such as vast consumption of energy resources and global warming effects due to the releasing of ozone-depleting coolants [2]. In return, annual rising of Earth's temperature and population growth are increasing the demand for cooling systems, and this destructive cycle is a threat for the future of Earth and living organisms security.

A novel method to reduce the usage of energy-consuming coolers is radiative cooling, a process by which an object passively loses heat through electromagnetic (EM) radiation [3]. According to Planck's law, every body having a temperature above absolute zero, emits EM radiation. For the black body at typical temperature of 300 K radiation peak occurs at wavelength around 9.7 μm, which stands inside the atmospheric transparency window ranging from wavelength 8 to 13 μm. Therefore, radiation emitted by terrestrial bodies in this range of wavelength can easily pass through the atmosphere and reach the space with a temperature around 3 K [4]. In other words, we can imagine that the terrestrial bodies are basically in thermal contact with the space. Following upon this concept, scientists have tried to design artificial structures, namely radiative coolers, to enhance this thermal contact [5], [6]. Practically, this enhancement results in temperature reduction of the radiative cooler, as has been reported in earlier studies [7], [8], [9], [10], [11], [12].

In achieving the radiative cooling property, two major optical characteristics are simultaneously required: 1) close to unity reflection in visible to near-infrared (near-IR) range (0.3–3 μm) and 2) close to unity emission in mid-IR range (8–13 μm) [3]. With both conditions happening, the temperature of radiative cooling structure can be reduced to reach to lower temperature but not necessarily below the ambient [12]. It is worth mentioning that for reaching to sub-ambient temperature, a radiative cooling structure which additionally has zero emission outside the atmospheric window is required [13], which is outside the scope of this work.

To realize the first condition, we can benefit from the properties of metals like Ag or Al. However, adding nano-pores into polymer substrate is an alternative way to reach high and diffuse reflectance in visible to near-IR wavelength range [10], [11]. To fulfill the second condition, it is common to utilize materials which their optical property has some extinction coefficient maxima within the atmospheric window [9], [10], [11], [12]. Therefore, any material having an extinction coefficient peak within the wavelength range of 8–13 μm is a potential candidate for using in radiative cooling structures.

In regards to architecture, several radiative cooling structures have been proposed including multilayered [7], [9], [14], periodic [12], [13], [15], nano-particle [8], [16], [17], [18], and porous polymer [10], [11] based structures. Multilayered structures consist of alternating layers of materials with different

Manuscript received 12 May 2023; revised 30 June 2023; accepted 6 July 2023. Date of publication 11 July 2023; date of current version 25 July 2023. *(Corresponding author: Majid Badieirostami.)*

Seyed Hossein Hosseini Biuki was with the School of Electrical and Computer Engineering, College of Engineering, University of Tehran, Tehran 14166-34793, Iran. He is now with the Department of Electrical Engineering, Sharif University of Technology, Tehran 11365-11155, Iran (e-mail: sh.hosseini@ee.sharif.edu).

Majid Badieirostami and Mahmoud Shahabadi are with the School of Electrical and Computer Engineering, College of Engineering, University of Tehran, Tehran 14166-34793, Iran (e-mail: mbadiei@ut.ac.ir; shahabad@ut.ac.ir).

Digital Object Identifier 10.1109/JPHOT.2023.3294442

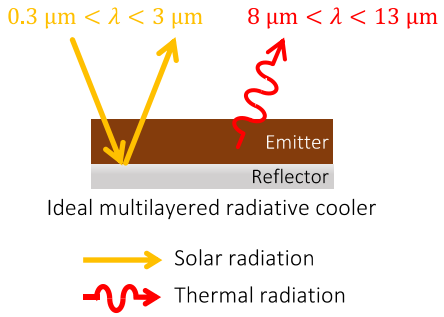

Fig. 1. Schematic of a multilayered radiative cooling structure composed of an emitter placed on top of a reflector layer.

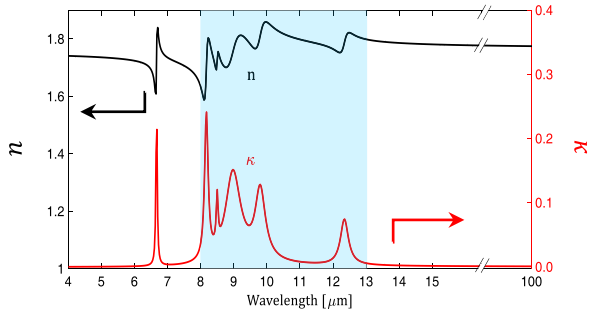

Fig. 2. Complex refractive index $(n - j\kappa)$ of SU-8 2025 extracted from the Lorentz-Drude model proposed in [21]. The transparency window of atmosphere is highlighted. The existence of multiple peaks in the imaginary part of the refractive index, makes SU-8 a good emitter (absorber) in this region and hence a good candidate for the emitter part of a radiative cooling structure.

thicknesses. The number and thickness of layers are optimized so to achieve thermal emittance in atmospheric window as well as reflectance in the visible to near-IR range. Although these structures are usually simple to fabricate in small scales, they are not suitable for mass production. For the periodic structures, the emissivity of a bulk intrinsic thermal radiator is enhanced by periodic patterning of an appropriate geometry, and then placed on top of a solar reflective layer. Manufacturability and reproducibility are yet the main concerns for the applicability of the periodic architectures. The nano-particle based structure is type of a metamaterial consisting of nano-particles of an intrinsic thermal emitter material randomly dispersed in a polymer host layer. Additionally, the high reflectance across solar wavelengths is achieved by a metal layer or a TiO_2 particle-doped polymer. Scalability in fabrication is the major advantage of this design. The porous polymers have recently attracted attentions due to their ability in eliminating metal usage. In these structures, some nano-pores are formed into the intrinsic thermal emitter polymer. The air voids emerged with random sizes and positions, backscatter the sun radiation and result in high diffuse reflectance from the structure. The major advantage of this architecture is flexibility which makes it suitable for coating on curved surfaces as fabrics.

The main goal of this study is to come up with an excellent emitter in the wavelength range of 8–13 μm where as well it is highly transparent across the solar wavelengths. The designed structure can be further placed on top of a normal near unity reflector made of Ag or Al to acheive a full radiative cooling architecture as schematically shown in Fig. 1.

II. The Proposed Structure

What we are proposing here as a radiative cooling structure is a microstructure patterned in SU-8 for high emissivity. SU-8 is a biocompatible photoresist commonly used in microelectromechanical systems (MEMS) industries. As can be seen in the following, SU-8 possesses excellent intrinsic EM properties appropriate for radiative cooling applications. SU-8 which is a highly transparent material in the visible and the near-IR shows negligible extinction coefficient [19], [20]. Thus, it has a minimal solar heating across the solar wavelengths. Moreover, according to a recent technical report, SU-8 has high extinction coefficient including multiple peaks in the thermal window, which determines its mid-IR properties [21]. Fig. 2 shows the complex refractive index $(n - j\kappa)$ of SU-8 2025 in the mid-IR region, where the refractive index was calculated using the Lorentz-Drude model presented in [21]. Moreover, for practical reasons in regards to microfabrication, SU-8 is the most favorite material in photolithography. This includes its excellent surface coating homogeneity as well as its mechanical and thermal stability through post-processing, which enables simple bonding and packaging for various applications [22].

Besides material, the structural shape also has significant impact on its absorption characteristics [23], e.g., by grooving an intrinsic absorptive (lossy) material its absorptivity and bandwidth are increased [24]. The pyramidal and wedge-shaped absorbers, extensively used in anechoic chambers for antenna measurements, are the well-known examples [25]. When irradiating the absorber, its V-grooved layer acts as a transition and provides a gradual matching from free space to the bottom of the absorber [26]. This results in minor reflections from the structure; hence, the incident wave is trapped in the lossy material and highly absorbed therein [26].

In this work, we investigated the surface grooving of SU-8 2025 to enhance the absorptivity (emissivity) of the intrinsic emitter to reach near unity emissivity in the wavelength range of 8–13 μm. Fig. 3 shows our proposed emitter structure comprising a one dimensional (1D) periodic layer of V-shaped parallel grooves coated on top of a substrate layer. For the substrate, we have chosen a lime glass slide since it is widely used and highly transparent across the solar wavelengths [27]. Four major design parameters, i.e., periodicity of SU-8 grooves (D), top groove width (W), groove angle (Θ), and SU-8 thickness (t_1) were involved to optimize the microstructure emissivity in wavelengths ranging from 8 - 13 μm. The thickness of the substrate (t_2) is set to 150 μm, typical of the glass slides used in the microfabrication, and the thickness of SU-8 layer is set to a typical value of 30 μm. It is worth mentioning that the emissivity of the SU-8 flat layer becomes nearly constant beyond this thickness. These two thicknesses are assumed fixed throughout this study.

For optimization purposes, there are some natural geometry consraints we have to consider. The top width groove (W) should be less than or equal to periodicity (D), and the thickness

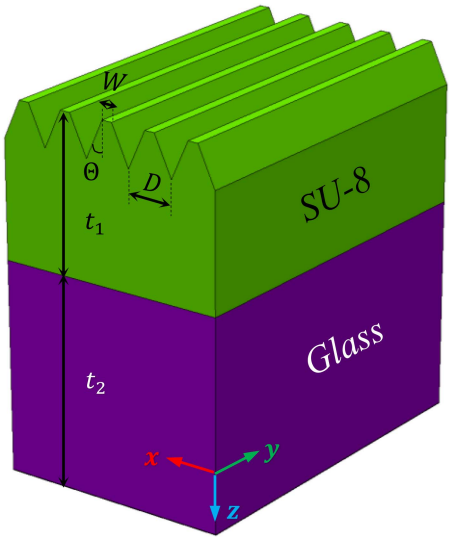

Fig. 3. Proposed emitter with high emissivity as the top part of a radiative cooling structure. The emitter is composed of a 1D periodic SU-8 layer coated on top of a common lime glass substrate ($t_1 = 30\ \mu$m, $t_2 = 150\ \mu$m).

of the SU-8 layer (t_1) should be greater than or equal to the grooves height, i.e., $(D - W)\cot(\Theta)/2$. In our simulations, the spectral complex refractive indices of SU-8 and glass are required and hence are taken from the perevious reports [21], [27].

III. Simulation Results and Discussion

We know that the ratio of radiation emitted from a structure at a specific temperature, at an arbitrary wavelength (λ), polarization (P), and direction (θ, φ) to the emitted energy from perfect emitter (black body) at the same condition, is defined as spectral directional emissivity, i.e., $\varepsilon_\lambda^P(\theta, \varphi)$. Hereafter, we call it briefly as emissivity. Our decision rule in the design procedure is based on the normal emissivity averaging over the wavelength range of 8–13 μm and over the s and p-polarizations, i.e., $\bar{\varepsilon}_{8-13}(0, 0)$. It is briefly referred to as $\bar{\varepsilon}_{8-13}$. According to Kirchhoff's law of thermal radiation, at steady state, i.e., thermodynamic equilibrium, the emissivity of an object is equal to its absorptivity for an incident plane wave with the four parameters listed above, i.e., $\alpha_\lambda^P(\theta, \varphi)$ [28]. Therefore, in order to analyze our V-grooved microstructure, we have to think of a way for absorption calculation. In this study, we have used a fast and accurate numerical full-wave method known as transmission-line formulation (TLF) [29]. This semi-analytical method is appropriate for determining the diffracted and transmitted modes of a multilayered photonic crystal (PC) as similarly outlined in Ref [30]. By knowing the diffraction and the transmission, the absorption may simply be calculated. Considering the V-grooved microstructure proposed here as a multilayered PC with a 1D periodicity in the xy-plane, we have subdivided the PC into N layers along the z-direction as shown in Fig. 4(a). The V-grooved part of the structure should be subdivided densely so to include the edge effects. Per our numerical calculations which will be explained further, $N = 22$ is sufficient to reach very small calculation error compared with the conventional finite element method (FEM) simulations.

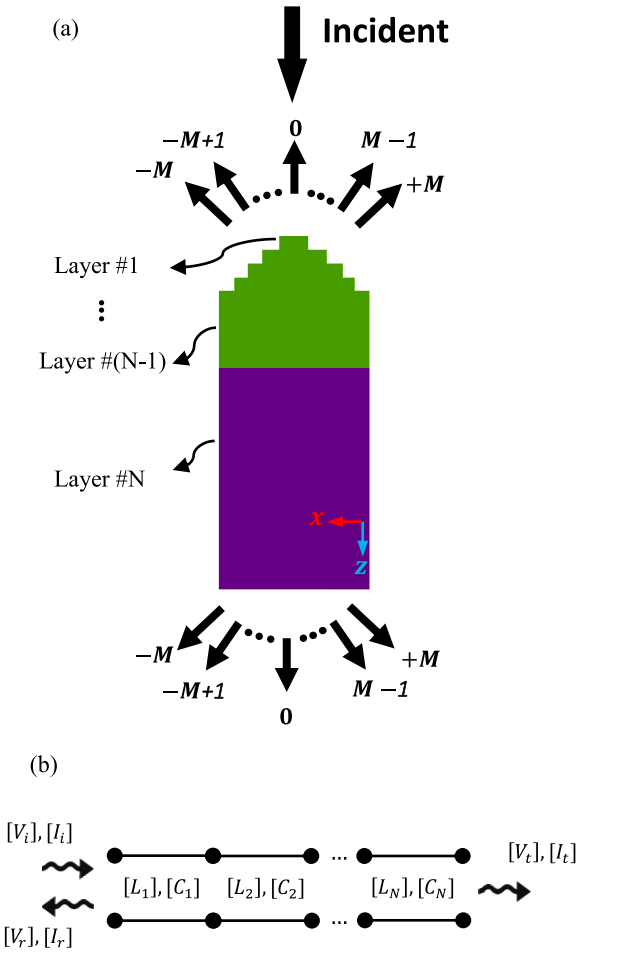

Fig. 4. TLF implementation for the V-grooved microstructure graphically represented with its unit cell. With the help of the TLF, absorptivity (emissivity) calculations for our V-grooved microstructure simply reduce to a circuit analysis of a multiconductor TL. (a) Shematic of the unit cell subdivided into N layers. In absorptivity calculation, the $2M + 1$ diffraction and transmission modes are considered. (b) Shematic of the multiconductor TLs as the equivalent circuit repersentation of the structure.

Briefly in TLF implementation, each layer is either homogeneous or periodic in the xy-plane, thus the complex permittivity function can respectively be expanded as either a constant function or a Fourier series of z-dependent coefficients. According to the Bloch theory, the total EM field propagating in each layer can be expressed as a superposition of multiple propagating modes in a pseudo-Fourier form. By appropriate matrix representation of EM fields and permittivity and then their substitution into Maxwell's equations, a coupled matrix equation for s (TE_z) polarization, i.e.,

$$\frac{d}{dz}\left([\mathcal{E}_y]\right) = -j\omega\ [L]\ \left(-[\mathcal{H}_x]\right) \tag{1}$$

$$\frac{d}{dz}\ \left(-[\mathcal{H}_x]\right) = -j\omega\ [C]\ \left([\mathcal{E}_y]\right) \tag{2}$$

is resulted for each layer, in which the $[\mathcal{E}_y]$ and $[\mathcal{H}_x]$ matrices are of $(2M + 1) \times 1$ dimensions consisting of y and x-complex

TABLE I
DIMENSIONS OF THE OPTIMIZED V-GROOVED MICROSTRUCTURE

D (μm)	W (μm)	Θ (°)	t_1 (μm)	$\bar{\varepsilon}_{8-13}$
9	1	20	30	99.47 %

amplitudes of electric and magnetic fields of the propagating modes, respectively. In the problem of plane wave incidence with direction (θ, φ), the m-th entry of the above matrices has the wave vector $\vec{k}_m = (k_x + \frac{2(m-M-1)\pi}{D})\,\hat{x} + k_y\,\hat{y} + k_{z,m}\hat{z}$, in which $k_x = k\,sin\theta\,cos\varphi$, $k_y = k\,sin\theta\,sin\varphi$, k is the wave vector of the incident wave, and $k_{z,m}$ is determined from the Helmholtz equation as,

$$k_{z,m}^2 + \left(\frac{2\,(m-M-1)\,\pi}{D} + k_x\right)^2 + k_y^2 = \left(\frac{2\pi}{\lambda}\right)^2 \tag{3}$$

in which λ is the wavelength of the incident wave. For each layer, the $[L]$ and $[C]$ matrices are specifically filled with the k_m's and the Fourier series coefficients of that same layer. It is to be noted that in $p\,(TM_z)$ polarization case, the resulted equations are the same as (1) and (2). In our calculation M is set to 5.

If one regards $[\mathcal{E}_y]$ and $-[\mathcal{H}_x]$ as line voltage and current, i.e., $[V]$ and $[I]$, respectively, these equations resemble those of an ideal multiconductor transmission line (TL). As illustrated in Fig. 4(b), the n-th layer could be modeled as a multiconductor TL with equivalent inductance and capacitance matrices, i.e., $[L_n]$ and $[C_n]$, and subsequently, the whole multilayered PC is modeled as coupled multiconductor TLs. Therefore, solving for the EM wave propagating inside the multilayered PC reduces to the circuit analysis of an equivalent multiconductor TL. Hence, finding the diffracted and transmitted field modes of the multilayered PC is equivalent to solve the reflection and transmission voltage and current matrices, i.e., $\{[V_r], [I_r]\}$ and $\{[V_t], [I_t]\}$, respectively. Thereafter, the total reflection (R), transmission (T) and subsequently, the absorption (A) of the structure is simply computed as,

$$R = \frac{\mathrm{Re}\left([V_r]^H\,[I_r]\right)}{\mathrm{Re}\left([V_i]^H\,[I_i]\right)} \tag{4}$$

$$T = \frac{\mathrm{Re}\left([V_t]^H\,[I_t]\right)}{\mathrm{Re}\left([V_i]^H\,[I_i]\right)} \tag{5}$$

$$A = 1 - R - T \tag{6}$$

where the $\{[V_i], [I_i]\}$ matrices are filled according to the incident s or p-polarized EM field. The H is the notation of Hermitian transpose.

Per the optimization results, the $\bar{\varepsilon}_{8-13}$ of the V-grooved microstructure exceeded 99.47%. The design parameters of the optimal structure are listed in Table I. Fig. 5 shows the calculated spectral emissivity of the optimized V-grooved microstructure for s and p polarizations using TLF method versus FEM simulation in COMSOL. Clearly, there is a very good agreement

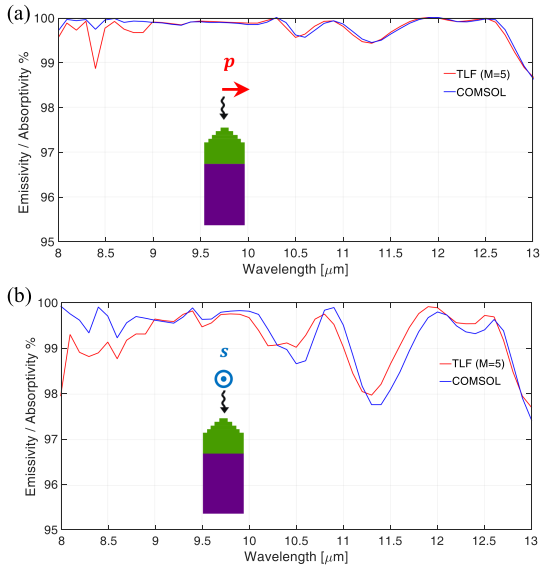

Fig. 5. Emissivity (absorptivity) of the optimized V-grooved microstructure with the dimensions listed in Table I for (a) p and (b) s- polarization. The TLF method (red) is compared against the FEM simulations in COMSOL (blue).

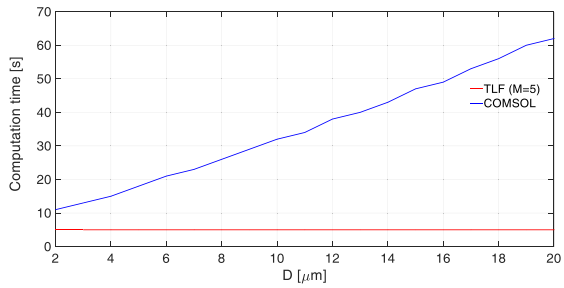

Fig. 6. Time spent for emissivity calculation of the V-grooved microstructure ($W = 1\,\mu$m, $\Theta = 20°$, $t_1 = 30\,\mu$m) for a single wavelength ($\lambda = 10\,\mu$m) versus period (D) in the TLF method (red) and in COMSOL simulation (blue). The structure was irradiated by a normal s-polarized plane wave.

between the two simulation results confirming the accuracy of our TLF numerical method.

To compare the computation speed of the TLF method versus COMSOL simulation, the period (D) of the optimized V-grooved microstructure was swept from 2 μm to 20 μm with 1 μm steps and for each case, the emissivity was calculated at a single wavelength ($\lambda = 10\,\mu$m). Both simulations were carried out on a personal computer with a typical Intel Core i5 CPU. Fig. 6 shows the computation time spent in each simulation. Obviously, increasing the size of the unit cell results in longer computation time for the FEM method due to larger mesh numbers, while in the TLF method the unit cell size has no effect in the computation time.

Next, we investigated the imapct of design parameters on the emissivity performance of the V-grooved microstructure. Considering the wavelength range of 8–13 μm and accounting for fabrication feasibility, we restricted W and D to a range of 1–25 μm with 1 μm steps. Fig. 7(a) and (b) show the averaged emissivity for the s and p-polarized radiation, respectively, from a V-grooved microstructure with arbitrary angle of $\Theta = 30°$.

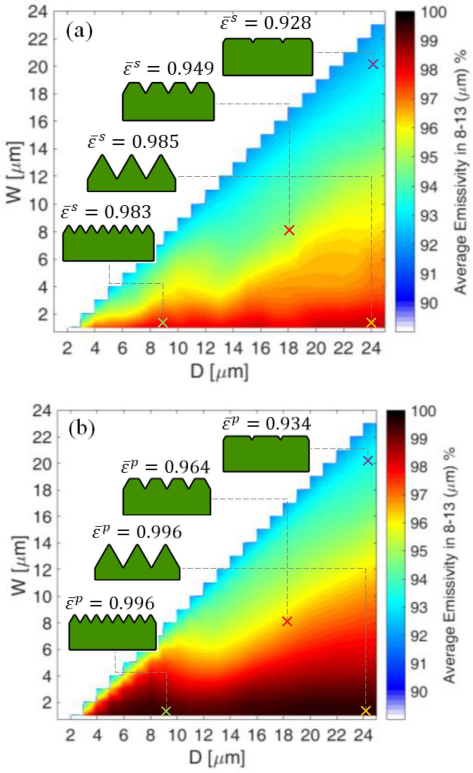

Fig. 7. Average emissivity from the V-grooved microstructure in the wavelength range of 8–13 μm with $\Theta = 30^\circ$ for (a) s and, (b) p-polarization. Each inset shows the structure for a specific point within the given range. The thickness of SU-8 layer (t_1) is fixed at 30 μm.

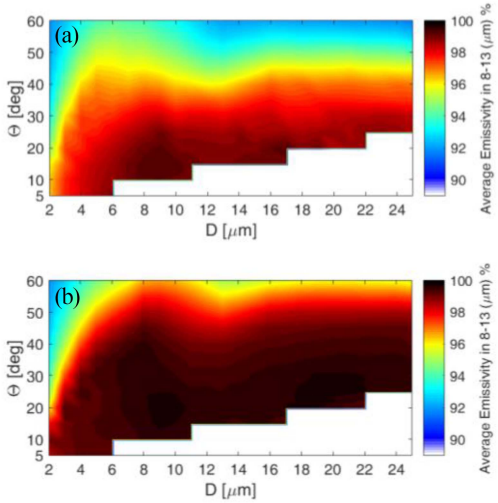

Fig. 8. Average emissivity from the V-grooved microstructure in the wavelength range of 8–13 μm with $W = 1$ μm for (a) s and, (b) p-polarization.

The white area of these plots corresponds to the violation of the geometry constraints mentioned earlier. The averaged emissivity for both polarizations improved significantly for $W \leq 2$ μm and $D \geq 4$ μm.

Further, we investigated the effect of groove angle on the averaged emissivity performance. By fixing $W = 1$ μm, the averaged emissivity is plotted versus D and Θ in Fig. 8. Θ is swept from 5° to 60° in steps of 5° and D has the same range as seen in Fig. 7. The averaged emissivity for both polarizations is significantly enhanced for Θ below 30° exceeding 99.4%. As the Θ increases, the surface grooving decreases which consequently results in lower emissivity.

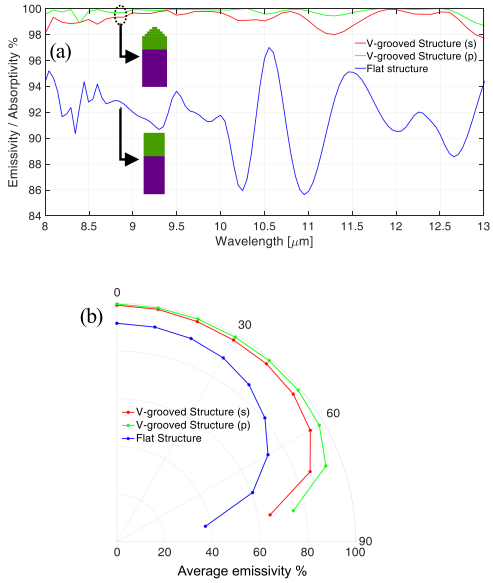

Fig. 9. (a) Spectral emissivity and, (b) directional average emissivity as a function of θ ($0^\circ \leq \theta \leq 80^\circ$) on the xz plane, i.e., $\varepsilon^{s/p}_{8-13}(\theta, 0)$, of the V-grooved microstructure with optimal parameters versus a flat SU-8 layer, both on top of a glass substrate ($t_1 = 30$ μm, $t_2 = 150$ μm).

To show the impact of the surface grooves in increasing the emissivity, we compared the emissivity of the optimized V-grooved microstructure versus a flat SU-8 layer, both placed on top of a glass substrate of the same thickness. As seen in Fig. 9(a), the average emissivity of the V-grooved structure is roughly 8% higher. In addition, the directional averaged emissivity of V-grooved structure is enhanced for both polarizations. To show this, the directional average emissivity on the xz plane as a function of θ ($0^\circ \leq \theta \leq 80^\circ$), i.e., $\varepsilon^{s/p}_{8-13}(\theta, 0)$, is plotted for the two structures (Fig. 9(b)).

To expose more details, the absorption rate, i.e., dP_A/dz was calculated. In the proposed network model, the absorption rate in the k-th layer (Fig. 10(a)) can be calculated as,

$$\frac{dP_A}{dz} = \frac{1}{2} \frac{\mathrm{Re}([V_k]^H [I_k] - [V_{k+1}]^H [I_{k+1}])}{z_{k+1} - z_k} \tag{7}$$

Then, the result of (7) is divided by the input power to give us the normalized absoprtion rate. This was calculated for both the optimized V-grooved microstructure and a flat SU-8 layer and is shown in Fig. 10(b). As can be seen, the absorptance in the grooved part ($z < z_V$) is enhanced compared against the flat counterpart. This reveals the role of surface grating in trapping the incident wave and consequently the rise in absorption rate. To verify the results, at each z_k the power loss density, i.e., $\frac{1}{4}\omega\varepsilon''_r\,\varepsilon_0\,|E|^2$, where $\varepsilon''_r = \mathrm{Im}((n - j\kappa)^2)$, was integrated on

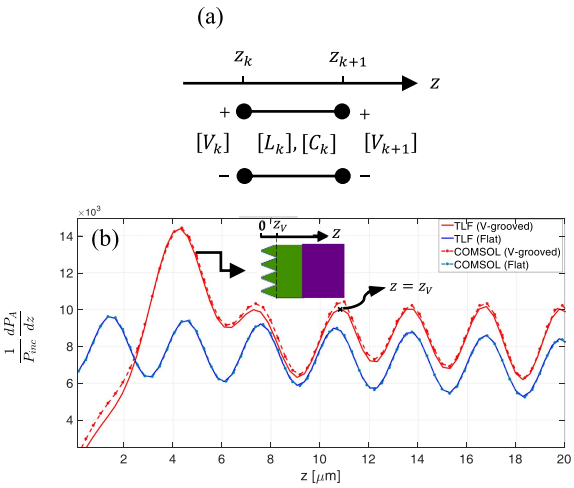

Fig. 10. (a) The k-th TL in the equivalent circuit repersentation of the proposed structure. (b) The absorption rate normalized to the incident power (P_{inc}) in the V-grooved microstructure compared against a flat SU-8 layer. The structure is irradiated by a normal s-polarized plane wave at $\lambda = 11$ μm.

the SU-8 cross-section line and then divided by the $(z_{k+1} - z_k)$. Clearly, there is an excellent agreement between the results.

IV. Conclusion

In this report the significance of SU-8 photoresist for the radiative cooling purposes is noticed for the first time. Then, a patterened microstructure made of SU-8 photoresist with extreme emissivity was proposed that seems very suitable for radiative cooling applications. In the design procedure, we engaged two concepts simultaneously. First, we used a material having an intrinsic emissivity (absorptivity) in the wavelength range of 8–13 μm. Second, we introduced a periodic V-grooved grating to adiabatically match the structure to free space. By considering fabrication feasibility of the structure, the effect of patterning parameters on the averaged emissivity was studied with TLF method. It is accurate enough though remarkably fast simulation method that provides us with the systematic design criteria for selection of the structure parameters. The most significant parameter is the top groove width (W). If W is minimized, the surface profile of the medium becomes sharper for the incident wave, resulting in lower reflection and higher absorption (emission). Finally, the structure was optimized for the average emissivity in the wavelength range of 8–13 μm, confirming its potential for reaching to an average emissivty greater than 99%. Therefore, we believe this structure can be considered as a near-thermal black body in the atmospheric window.

References

[1] M. N. Bahadori, "Passive cooling systems in Iranian architecture," *Sci. Amer.*, vol. 238, no. 2, pp. 144–155, Feb. 1978.

[2] B. O. Bolaji and Z. Huan, "Ozone depletion and global warming: Case for the use of natural refrigerant—A review," *Renewable Sustain. Energy Rev.*, vol. 18, pp. 49–54, Feb. 2013, doi: 10.1016/j.rser.2012.10.008.

[3] D. Zhao et al., "Radiative sky cooling: Fundamental priciples, materials, and applications," *Appl. Phys. Rev.*, vol. 6, no. 2, Apr. 2019, Art. no. 021306, doi: 10.1063/1.5087281.

[4] S. Buddhiraju, P. Santhanam, and S. Fan, "Thermodynamic limits of energy harvesting from outgoing thermal radiation," *Proc. Nat. Acad. Sci.*, vol. 115, no. 16, pp. E3609–E3615, Apr. 2018.

[5] S. Catalanotti, V. Cuomo, G. Piro, D. Ruggi, V. Silvestrini, and G. Troise, "The radiative cooling of selective surfaces," *Sol. Energy*, vol. 17, no. 2, pp. 83–89, May 1975, doi: 10.1016/0038-092X(75)90062-6.

[6] C. G. Granqvist and A. Hjortsberg, "Radiative cooling to low temperatures: General considerations and application to selectively emitting SiO films," *J. Appl. Phys.*, vol. 52, no. 6, pp. 4205–4220, Jun. 1981, doi: 10.1063/1.329270.

[7] P. Raman, M. A. Anoma, L. Zhu, E. Rephaeli, and S. Fan, "Passive radiative cooling below ambient air temperature under direct sunlight," *Nature*, vol. 515, no. 7528, pp. 540–544, Nov. 2014, doi: 10.1038/nature13883.

[8] Y. Zhai et al., "Scalable-manufactured randomized glass-polymer hybrid metamaterial for daytime radiative cooling," *Science*, vol. 355, no. 6329, pp. 1062–1066, Feb. 2017, doi: 10.1126/science.aai7899.

[9] J. Kou, Z. Jurado, Z. Chen, S. Fan, and A. J. Minnich, "Daytime radiative cooling using near-black infrared emitters," *Amer. Chem. Soc. Photon.*, vol. 4, no. 3, pp. 626–630, Feb. 2017, doi: 10.1021/acsphotonics.6b00991.

[10] J. Mandal et al., "Hierarchically porous polymer coatings for highly efficient passive daytime radiative cooling," *Science*, vol. 362, no. 6412, pp. 315–319, Sep. 2018, doi: 10.1126/science.aat9513.

[11] D. Li et al., "Scalable and hierarchically designed polymer film as a selective thermal emitter for high-performance all-day radiative cooling," *Nature Nanotechnol.*, vol. 16, no. 2, pp. 153–158, Nov. 2021, doi: 10.1038/s41565-020-00800-4.

[12] M. Gao et al., "Approach to fabricating high-performance cooler with near-ideal emissive spectrum for above-ambient air temperature radiative cooling," *Sol. Energy Mater. Sol. Cells*, vol. 200, no. 1, Sep. 2019, Art. no. 110013, doi: 10.1016/j.solmat.2019.110013.

[13] E. Rephaeli, A. Raman, and S. Fan, "Ultrabroadband photonic structures to achieve high-performance daytime radiative cooling," *Nano Lett.*, vol. 13, no. 4, pp. 1457–1461, Mar. 2013, doi: 10.1021/nl4004283.

[14] M. A. Kecebas, M. P. Menguc, A. Kosar, and K. Sendur, "Spectrally selective filter design for passive radiative cooling," *J. Opt. Soc. Amer. B*, vol. 37, no. 4, pp. 1173–1182, Mar. 2020, doi: 10.1364/JOSAB.384181.

[15] D. Lee et al., "Sub-ambient daytime radiative cooling by silica-coated porous anodic aluminum oxide," *Nano Energy*, vol. 79, Jan. 2021, Art. no. 105426, doi: 10.1016/j.nanoen.2020.105426.

[16] D. Chae et al., "Spectrally selective nanoparticle mixture coating for passive daytime radiative cooling," *Amer. Chem. Soc. Appl. Mater. Interfaces*, vol. 13, pp. 21119–21126, Apr. 2021, doi: 10.1021/acsami.0c20311.

[17] Z. Huang and X. Ruan, "Nanoparticle embedded double-layer coating for daytime radiative cooling," *Int. J. Heat Mass Transfer*, vol. 104, no. 1, pp. 890–896, Jan. 2017, doi: 10.1016/j.ijheatmasstransfer.2016.08.009.

[18] X. P. Zhang, L. W. Yang, F. Q. Wang, Z. M. Cheng, and H. X. Liang, "Wrinkled surface microstructure for enhancing the infrared spectral performance of radiative cooling," *Opt. Exp.*, vol. 29, no. 8, pp. 11416–11432, Apr. 2021, doi: 10.1364/OE.418650.

[19] O. P. Parida and N. Bhat, "Characterization of optical properties of SU-8 and fabrication of optical components," in *Proc. Int. Conf. Opt. Photon.*, 2009, pp. 4–7.

[20] Kayaku Advanced Materials, "SU-8 2000 Permanent Negative Epoxy Photoresist," 2021. [Online]. Available: https://kayakuam.com/wp-content/uploads/2022/04/KAM-SU-8-2000-2025-2100-Datasheet-4.9.21-final.pdf

[21] E. Motaharifar, R. G. Pierce, R. Islam, R. Henderson, J. W. P. Hsu, and M. Lee, "Broadband terahertz refraction index dispersion and loss of polymeric dielectric substrate and packaging materials," *J. Infrared, Millimeter, Terahertz Waves*, vol. 39, no. 1, pp. 93–104, Sep. 2018, doi: 10.1007/s10762-017-0444-4.

[22] J. S. Lee and S. S. Lee, "Fabrication of a freestanding micro mechanical structure using electroplated thick metal with a HAR SU-8 mold," *Microsystem Technol.*, vol. 15, pp. 287–296, Oct. 2009, doi: 10.1007/s00542-008-0709-x.

[23] A. Sentenac and J. J. Greffet, "Design of surface microrelief with selective radiative properties," *Int. J. Heat Mass Transfer*, vol. 37, no. 4, pp. 553–558, Mar. 1994, doi: 10.1016/0017-9310(94)90127-9.

[24] H. Severin, "Nonreflecting absorbers for microwave radiation," *Inst. Radio Eng. Trans. Antennas Propag.*, vol. 4, no. 3, pp. 385–392, Jul. 1956, doi: 10.1109/TAP.1956.1144419.

[25] H. Nornikman, P. J. Soh, A. A. H. Azremi, and M. S. Anuar, "Performance simulation of pyramidal and wedge microwave absorbers," in *Proc. 3rd Asia Int. Conf. Modelling Simul.*, 2009, pp. 649–654.

[26] I. Ctalkaya and S. Kent, "An optimized microwave absorber geometry based on wedge absorber," *Appl. Comput. Electromagnetics Soc. J.*, vol. 32, no. 7, pp. 621–627, Jul. 2017.

[27] M. Rubin, "Optical properties of soda lime silica glasses," *Sol. Energy Mater.*, vol. 12, no. 4, pp. 275–288, Oct. 1985, doi: 10.1016/0165-1633(85)90052-8.

[28] T. L. Bergman, A. S. Lavine, F. P. Incropera, and D. P. Dewitt, "Radiation: Processes and properties," in *Fundamentals of Heat and Mass Transfer*, 7th ed. Hoboken, NJ, USA: Wiley, 2011.

[29] M. Shahabadi, S. Atakaramians, and N. Hojjat, "Transmission line formulation for the full-wave analysis of two-dimensional dielectric photonic crystals," *IEE Proc. Sci. Meas. Technol.*, vol. 151, no. 5, pp. 327–334, Sep. 2004, doi: 10.1049/ip-smt:20040819.

[30] H. Neshasteh, A. Mataji-Kojouri, S.-A. Akbarzadeh-Jahromi, and M. Shahabadi, "A hybrid photonic-plasmonic sensing platform for differentiating background and surface interactions using an array of metal-insulator-metal resonators," *IEEE Sensors J.*, vol. 16, no. 6, pp. 1621–1627, Mar. 2016, doi: 10.1109/JSEN.2015.2503378.